An OpenFOAM Solver for Criticality Safety Assessment in Dynamic Compression Events

Eric Cervi, Stefano Lorenzi, Lelio Luzzi, Antonio Cammi

Politecnico di Milano, Via La Masa 34, 20156, Milan, Italy

eric.cervi@polimi.it, stefano.lorenzi@polimi.it, lelio.luzzi@polimi.it, antonio.cammi@polimi.it

INTRODUCTION

The purpose of this summary is to present a multi-physics simulation tool for computational criticality safety evaluations. Typical design-basis events that should be considered for impact on reactivity safety are fires, energetic events such as explosions, seismic events, tornado, wind and hurricane events, external floods and precipitation events and aircraft crash events [1]. In these conditions, materials exhibit a large range of responses, requiring the development of different material models for a correct simulation of all these accidents.

In this regard, a coupled neutronics and thermal-mechanics OpenFOAM [2] solver is under development at Politecnico di Milano. The thermal-mechanics module implements balance equations for mass, momentum and energy, a dynamic mesh and different material response models (among which a hydrodynamic model for strong shock compression of solids [3]), to describe both small and large deformations. On the other hand, a multi-group SP3 transport model is developed for neutronics, in order to provide an accurate description of the neutron flux in small, strongly leakage-dominated systems.

In more details, the present work focuses on criticality safety assessment of solid fissile materials during strong dynamic compression events, such as chemical explosions. To this aim, the hydrodynamic material response model is presented, to simulate shockwave propagation in solid multiplying media and its effect on reactivity. In this regard, multi-physics constitutes a useful approach to address this complex problem, providing a way to describe all the physics that come into play as well as the coupling between them.

Different shock physics codes are currently available (see, e.g., [4,5]) but, according to present literature, none of them implements a neutronics module. The aim of the present summary is to fill this gap, presenting a multi-physics solver coupling neutron transport and shock physics in the same simulation environment, for nuclear criticality safety applications.

Different case studies are proposed to quantitatively verify the developed models and to demonstrate the potentialities of the multi-physics solver.

Modelling approach

In this section, the structure of the solver and the multi-physics coupling strategy are described. At each time step, the systems neutronics and thermal-mechanics are solved in two different iterative cycles, as shown in Figure 1. In addition, external iterations between the neutronics and thermal-mechanics cycles are performed, to solve the non-linearities between the two physics. The developed models for the system neutronics and thermal-mechanics are described in the following sections.

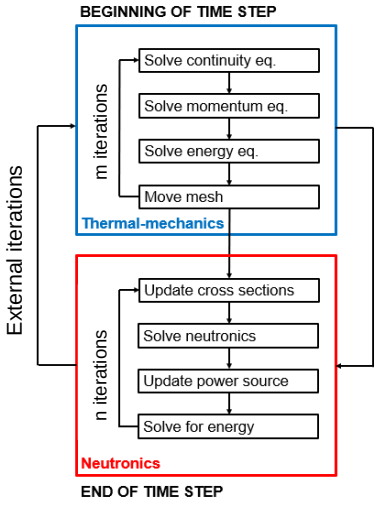

Fig. 1. Solver structure and coupling strategy.

The thermal-mechanics module

In the thermal-mechanics cycle, the mass, momentum and energy balance equations for a continuum medium are solved:

$$\frac{\partial \rho}{\partial t} + \nabla \cdot [\rho(\boldsymbol{u} - \boldsymbol{w})] = 0 \tag{1}$$

$$\frac{\partial (\rho \boldsymbol{u})}{\partial t} + \nabla \cdot [\rho \boldsymbol{u}(\boldsymbol{u} - \boldsymbol{w})] = \nabla \cdot \underline{\underline{\boldsymbol{\tau}}} - \nabla p + \boldsymbol{b} \tag{2}$$

$$\frac{\partial (\rho h)}{\partial t} + \nabla \cdot [\rho h(\boldsymbol{u} - \boldsymbol{w})] = k\nabla^2 T + \frac{Dp}{Dt} + \dot{q} \tag{3}$$

After convergence of the thermal-mechanics solution, the dynamic mesh is moved in order to catch the material deformations. The balance equations are written in an Arbitrary Lagrangian-Eulerian (ALE) form: the mesh vertices can be moved with an arbitrary velocity $\boldsymbol{w}$, to preserve the mesh quality in case of strong distortions. This velocity is included in the avvective terms of the equations in order to preserve the balances. In this work, a pure Lagrangian approach is adopted, assuming $\boldsymbol{u} = \boldsymbol{w}$, since mesh distortions are not an issue in the simple cases considered through the summary. The main advantage of the

Lagrangian approach is a more accurate description of surface motion, which is crucial for a correct evaluation of deformation feedbacks on neutronics. Nevertheless, the ALE formulation can be useful for future simulations involving more significant mesh distortions.

A constitutive model for the material response is also required to close the thermal-mechanics problem, in addition to Eqs. (1) to (3).

The neutronics module

An SP3 transport module is implemented for neutronics. Compared to diffusion approaches, a transport model is more suitable for the description of small systems, in which neutron leakages have a strong feedback on reactivity. In this regard, the SP3 equations are selected as a trade-off between model accuracy and computational cost:

$$\frac{1}{v_i}\frac{\partial \Phi_{0,i}}{\partial t} = \nabla \cdot D_{0,i}\nabla\Phi_{0,i} - \Sigma_{r,i}\left(\Phi_{0,i} - 2\varphi_{2,i}\right) + S_{n,i}(1-\beta)\chi_{p,i} + S_d\chi_{d,i} + S_{s,i} + \frac{2}{v_i}\frac{\partial \varphi_{2,i}}{\partial t} \quad (4)$$

$$\frac{9}{5}\frac{1}{v_i}\frac{\partial \varphi_{2,i}}{\partial t} = \nabla \cdot D_{2,i}\nabla\varphi_{2,i} - \Sigma_{t2,i}\varphi_{2,i} + \frac{2}{5}\Sigma_{r,i}\left(\Phi_{0,i} - 2\varphi_{2,i}\right) - \frac{2}{5}S_{n,i}(1-\beta)\chi_{p,i} - \frac{2}{5}S_d\chi_{d,i} - \frac{2}{5}S_{s,i} + \frac{2}{5}\frac{1}{v_i}\frac{\partial \Phi_{0,i}}{\partial t} \quad (5)$$

where S_n, S_s and S_d are the fission neutron, scattering neutron and delayed neutron source terms, respectively, while:

$$\Phi_{0,i} = \varphi_{0,i} + 2\varphi_{2,i} \quad (6)$$

$$D_{0,i} = \frac{1}{\Sigma_{tr,i}},\quad \Sigma_{t2,i} = \Sigma_{t,i} - \Sigma_{sn2,ii},\quad D_{2,i} = \frac{9}{35}\frac{1}{\Sigma_{t,i} - \Sigma_{sn3,ii}} \quad (7)$$

Cross sections are evaluated by assuming a logarithmic dependence on temperature and a linear dependence on density:

$$\Sigma_{i,j} = \left[\Sigma^o_{i,j} + A_{i,j} log\frac{T_{fuel}}{T_{ref}}\right]\frac{\rho_{fuel}}{\rho_{ref,fuel}} \quad (8)$$

Balance equations for precursor densities are implemented into the neutronics model:

$$\frac{\partial c_k}{\partial t} + \nabla \cdot [c_k(\boldsymbol{u} - \boldsymbol{w})] = \beta_k \sum_i \bar{\nu}\Sigma_{f,i}\varphi_i - \lambda_k c_k \quad (9)$$

A power iteration routine, based on the *k*-eigenvalue method, is also implemented for the estimation of the multiplication factor. Several verifications have been carried out by the authors to assess the correct implementation of the neutronics module.

The hydrodynamic model

In this section, a material model for strong shockwave compression of solids is presented. Above pressures of 5-10 GPa, the shear stresses become negligible and the solid response to shock compression is similar to that of an inviscid, compressible fluid [3]. Note that 5 GPa or larger pressures are attainable in strong energetic events such as chemical explosions, which are some of the design-basis accidents that need to be considered for impact on criticality safety [1].

Within this approximation, the *"shock conditions"*, expressing integral mass, momentum and energy balance across the shock front, become [6]:

$$[\rho]u_s = [\rho u] \quad (10)$$

$$[\rho u]u_s = [\rho u^2 + p] \quad (11)$$

$$\left[\rho\left(e + \frac{1}{2}u^2\right)\right]u_s = \left[\rho\left(e + \frac{1}{2}u^2\right)u + pu\right] \quad (12)$$

where the notation [] indicates the difference between the upstream and downstream conditions with respect to the shock front. Elaborating Eqs. (11) and (12), the important Rankine-Hugoniot relation can be derived:

$$e_2 - e_1 = \frac{1}{2}(p_1 + p_2)(v_1 - v_2) \quad (13)$$

where the indices 1 and 2 indicate the upstream and downstream conditions, respectively.

Finally, combining Eq. (13) with an equation of state $e = f(p, v)$, the Hugoniot curve, or *shock adiabat*, can be obtained. The Hugoniot curve relates the initial and the possible end states of a material crossed by a shockwave. Thanks to the shock conditions, the Hugoniot curve can be expressed in different forms. Among these, the $u - U_s$ (material velocity – Lagrangian shock velocity) curve is one of the most commonly used to represent experimental data. Above pressures of 5-10 GPa, the $u - U_s$ Hugoniot assumes a simple linear form [3]:

$$U_s = C_B + S|u| \quad (14)$$

where C_B and S are material constants.

When the hydrodynamic approximation holds, a solid can be described with the $p - v - e$ Mie-Grüneisen equation of state [3]:

$$p - p_H = \frac{\gamma(v)}{v}(e - e_H) \quad (15)$$

where p_H and e_H are the pressure and internal energy lying on a Hugoniot curve, while γ is the Grüneisen parameter. Once C_B and S are known from experimental measurements, p_H and e_H can be determined using the shock conditions. Moreover, the Grüneisen parameter can be estimated as [6]:

$$\gamma(v) = \left(\frac{v}{v_0} - 1\right)\left(S^2 - \frac{1}{3}S + \frac{5}{9}\right) + (2S - 1) \qquad (16)$$

Therefore, C_B and S are the input parameters required by the model to write the Mie-Grüneisen equation of state.

RESULTS

Verification of the hydrodynamic model

In this section, the correct implementation of the hydrodynamic model is verified. The speed of shockwaves of different strength, propagating in metallic uranium, is calculated with the multi-physics solver in a 1D domain and is compared to the speed predicted by the experimental $u - U_s$ Hugoniot curve ($C_B = 2487\ m/s$ and $S = 1.539$ [7]) for each value of the pressure. Results for pressures from 10 to 80 GPa are listed in Table I.

TABLE I. Comparison between calculated and experimental Hugoniot shock speeds for p from 10 to 80 GPa.

Pressure	Calculated shock speed	Hugoniot shock speed	Relative difference
10 GPa	2764 m/s	2780 m/s	-0.6%
20 GPa	2976 m/s	3028 m/s	-1.7%
30 GPa	3188 m/s	3249 m/s	-1.9%
40 GPa	3336 m/s	3451 m/s	-3.3%
50 GPa	3484 m/s	3637 m/s	-4.2%
60 GPa	3624 m/s	3811 m/s	-4.9%
70 GPa	3758 m/s	3975 m/s	-5.4%
80 GPa	3892 m/s	4132 m/s	-5.8%

Excellent agreement is obtained between the calculated and the Hugoniot shock speeds over the whole investigated pressure range. The authors also verified that shock conditions, Eqs. (10) to (12), are satisfied in the entire range.

The multi-physics coupling

In this section, two simple test cases are considered to demonstrate the multi-physics coupling between shockwave propagation and neutronics. Note that these case studies are not representative of real-life accidents. The definition of design-basis events is not in the scope of the present summary. The cases are selected to show:

i) the coupling between neutronics and shockwave propagation;
ii) the capability of the solver to reproduce typical shock physics phenomena, such as the interaction between two crossing shocks and the amplification of a converging shockwave;
iii) the capability of the solver to deal with both subcritical and supercritical events.

The first case study consists of a 1D metallic uranium infinite slab, enriched at 95% in ^{235}U, with 6.5 cm thickness. A 30 GPa pressure step is applied at both sides of the slab at $t = 0$. The resulting pressure and fission rate profiles for $t = 6\ \mu s$ and $t = 12\ \mu s$ are shown in Figure 2.

The shape of the two crossing shocks is reflected in the fission rate profile, clearly showing the coupling between the two physics. The multiplication factor, with initial value $k = 0.98329$, does not change during the transient, indicating that the system remains subcritical. In fact, due to the 1D slab geometry, the external surface is not reduced by the shock compression. Thus, neutron leakages and, as a consequence, reactivity, are not significantly affected by this event.

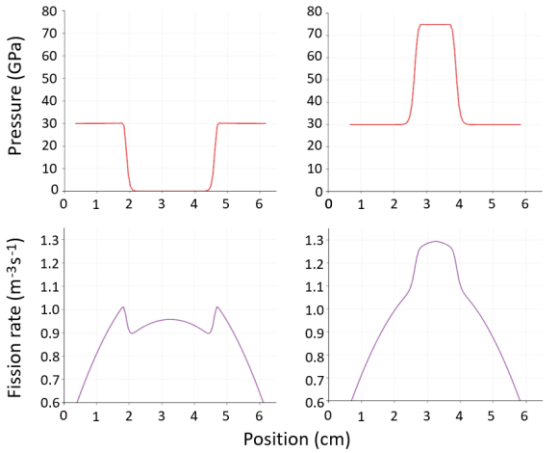

Fig. 2. Pressure and fission rate profiles in the slab at $t = 6\ \mu s$ (left) and $t = 12\ \mu s$ (right). The domain shrinks as time goes on, due to the motion of the computational mesh.

The second case study consists of a metallic uranium infinite cylinder, with 6 cm radius and same enrichment of the 1D slab. The initial multiplication factor of this system is $k = 0.97911$. At $t = 0$, a 30 GPa pressure step is applied to the lateral surface of the cylinder. The pressure and fission rate profiles at $t = 8\ \mu s$ and $t = 16\ \mu s$ are shown in Figure 3. Note that the wave front pressure increases as the shockwave converges to the axis of the cylinder.

Unlike the 1D slab, this case is strongly supercritical. The fission rate increases of 27 decades between $t = 8\ \mu s$ and $t = 16\ \mu s$. In particular, at $t = 16\ \mu s$, the multiplication factor, evaluated with the power iteration routine implemented in the neutronics module, is $k = 1.06520$. Due to the heating produced by fission power, the pressure in the central region of the cylinder increases before the arrival of the shockwave.

While in the 1D slab the surface area does not change with compression, in the cylinder case the external surface is significantly reduced by the converging shock, leading to a decrease of neutron leakages and, as a consequence, to a strong reactivity increase.

Hence, even if the initial multiplication factor and the surface pressure of the two cases are similar, completely different transients are observed following dynamic compression, due to the different shapes of the considered systems.

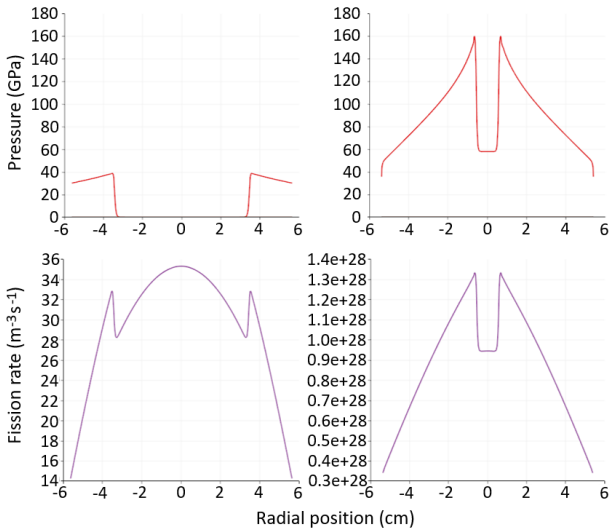

Fig. 3. Pressure and fission rate profiles in the cylinder at $t = 8\ \mu s$ (left) and $t = 16\ \mu s$ (right).

Conclusions

The present solver may represent a useful tool for criticality safety assessment in case of strong dynamic compression events. Thanks to the multi-physics modelling approach, both neutronics and shock-physics can be described in the same simulation environment, without requiring coupling interfaces between different codes. The solver has the capability to simulate both subcritical and supercritical events, highlighting the impact of the system shape on criticality during dynamic compressions.

Development of models for the analysis of high velocity impact events may be an interesting path for future research. More in general, the present solver can be coupled with other modules available in the OpenFOAM toolkit, to simulate other events (e.g., fire, sloshing of liquid tanks, etc.) that may have an impact on reactivity.

NOMENCLATURE

Latin symbols

A	Temperature coefficient, m^{-1}
$\boldsymbol{b}$	Body force, kg m^{-2} s^{-2}
c	Precursor density, m^{-3}
e	Internal energy, J kg^{-1}
h	Enthalpy, J kg^{-1}
k	Thermal conductivity, J m^{-1} K^{-1}
p	Pressure, Pa
$\dot{q}$	Power source, J s^{-1} m^{-1}
t	Time, s
T	Temperature, K
$\boldsymbol{u}$	Material velocity, m s^{-1}
u_S	Eulerian shock velocity, m s^{-1}
U_S	Lagrangian shock velocity, m s^{-1}
v	Specific volume, m^3 kg^{-1}
v_o	Specific volume at zero compression, m^3 kg^{-1}
v_i	Neutron velocity, m s^{-1}
$\boldsymbol{w}$	Arbitrary mesh velocity, m s^{-1}

Greek symbols

β	Delayed neutron fraction, -
γ	Grüneisen parameter, -
λ	Precursor decay constant, s^{-1}
$\bar{\nu}$	Average neutrons per fission, -
φ_o	Neutron flux, m^{-2} s^{-1}
φ_2	Second neutron flux moment,
ρ	Density, kg m^{-3}
Σ	Macroscopic cross section m^{-1}
$\underline{\underline{\boldsymbol{\tau}}}$	Stress tensor, Pa
χ	Neutron yield, -

Subscripts

d	Delayed
f	Fission
H	Hugoniot
p	Prompt
r	Removal
s	Scattering
sn	Inelastic scattering
t	Total
tr	Transport

REFERENCES

1. DOE Technical Standard, Preparing critical safety evaluations at department of energy nonreactor facilities (2017).
2. OpenFOAM documentation available at http://www.openfoam.org/docs/.
3. Davison, L., Fundamentals of Shock Wave Propagation in Solids, Springer-Verlag Berlin Heidelberg (2008).
4. McGlaun, J.M., Thompson, S.L., 1990. CTH: A three-dimensional shock wave physics code, International Journal of Impact Engineering 10, 351-360.
5. Summers, R.M., Peery, J.S., Wong, M.W., Herten Jr., E.S., Trucano, T.G., Chhabildas, L.C., 1997. Recent progress in ALEGRA development and application to ballistic impacts, International Journal of Impact Engineering 20, 779-788.
6. Grodzka P.G., Gruneisen parameter study, Lockheed Missiles and Space Company (1967).
7. Isbell, W.M., Shipman, F.H., Jones, A.H., Hugoniot equation of state measurements for eleven materials to five Megabars, Materials & Structures Laboratory Manufactory Development, General Motor Corporation (1971).